On Near-Field *w*-Projection for Radio Interferometric Imaging

JOSEPH LAZIO

Radio/Infrared/Optical Sensors Branch
Remote Sensing Division

May 12, 2009

REPORT DOCUMENTATION PAGE

1. REPORT DATE *(DD-MM-YYYY)*	2. REPORT TYPE	3. DATES COVERED *(From - To)*
12-05-2009	NRL Memorandum Report	December 2008 – March 2009

4. TITLE AND SUBTITLE

On Near-Field w-Projection for Radio Interferometric Imaging

5a. CONTRACT NUMBER
K448184

5b. GRANT NUMBER

5c. PROGRAM ELEMENT NUMBER

6. AUTHOR(S)

Joseph Lazio

5d. PROJECT NUMBER

5e. TASK NUMBER
2009-007

5f. WORK UNIT NUMBER
72-8272-A9-5

7. PERFORMING ORGANIZATION NAME(S) AND ADDRESS(ES)

Naval Research Laboratory
4555 Overlook Avenue, SW
Washington, DC 20375-5320

8. PERFORMING ORGANIZATION REPORT NUMBER

NRL/MR/7210--09-9173

9. SPONSORING / MONITORING AGENCY NAME(S) AND ADDRESS(ES)

SAF/FMBIB-AFOY
P.O. Box 14200
Washington, DC 20044-4200

10. SPONSOR / MONITOR'S ACRONYM(S)

11. SPONSOR / MONITOR'S REPORT NUMBER(S)

12. DISTRIBUTION / AVAILABILITY STATEMENT

Approved for public release; distribution is unlimited.

13. SUPPLEMENTARY NOTES

14. ABSTRACT

   This paper serves to elucidate the mathematical steps needed to apply near-field imaging over a significant (angular) area of regard, with specific application to the receiving sites of the Air Force Space Surveillance System (AFSSS, "Space Fence"). Cornwell has developed the mathematical formalism to merge near-field imaging with imaging over a wide field of view. The traditional far-field, narrow field-of-view imaging developed in radio astronomy can be extended to wide fields of view by taking into account the three-dimensional nature of the receiving array (the so-called "w term"), leading to a method called "w-projection." This w-projection method has the effect of retaining a Fresnel term in the imaging process, and Cornwell sketched how this w-projection might also be applicable to near-field imaging. For the Space Fence receiving sites, the near field is located at an altitude of approximately 1000 km. I illustrate how a near-field, w-projection imaging could be implemented for determining the direction cosines of radar reflections from a system like the Space Fence.

15. SUBJECT TERMS

Radio interferometry
Air Force Space Surveillance System

16. SECURITY CLASSIFICATION OF:			17. LIMITATION OF ABSTRACT	18. NUMBER OF PAGES	19a. NAME OF RESPONSIBLE PERSON
a. REPORT	**b. ABSTRACT**	**c. THIS PAGE**	UL	14	Joseph Lazio
Unclassified	Unclassified	Unclassified			**19b. TELEPHONE NUMBER** *(include area code)* (202) 404-6329

EXECUTIVE SUMMARY

This paper serves to elucidate the mathematical steps needed to apply near-field imaging over a significant (angular) area of regard, with specific application to the receiving sites of the Air Force Space Surveillence System (AFSSS, "Space Fence"). Cornwell has developed the mathematical formalism to merge near-field imaging with imaging over a wide field of view. The traditional far-field, narrow field-of-view imaging developed in radio astronomy can be extended to wide fields of view by taking into account the three-dimensional nature of the receiving array (the so-called "w term"), leading to a method called "w-projection." This w-projection method has the effect of retaining a Fresnel term in the imaging process, and Cornwell sketched how this w-projection might also be applicable to near-field imaging. For the Space Fence receiving sites, the near field is located an altitude of approximately 1000 km. I illustrate how a near-field, w-projection imaging could be implemented for determining the direction cosines of radar reflections from a system like the Space Fence.

ON NEAR-FIELD W-PROJECTION FOR RADIO INTERFEROMETRIC IMAGING

1. BACKGROUND

In traditional radio astronomical interferometric observations of celestial sources outside the solar system, imaging can be performed under the far-field approximation (Thompson, Moran, & Swenson, 1986, Chapter 3). For objects within the solar system, however, *near field* imaging may be required. Specific examples from radio astronomy include Very Long Baseline Observations of radar returns from near-Earth objects (Black et al., 2005). Although various techniques were developed to handle *near-field* imaging have been developed, we believe that Carter (1988) was the first to place these on a firm mathematical footing. In particular, Carter (1988) distinguished between the near-field of the *array* and the near-field of the *source*.

While radio astronomical imaging of objects in the solar system may require taking near-field effects into account, the density of objects in the sky is sufficiently low that searches at radio wavelengths (with the sensitivities provided by current instrumentation) are not practical. Consequently, only a small region of the sky surrounding the target object needs to be imaged. In contrast, one of the operational modes for a space situational awareness array, such as the Air Force Space Surveillance System,[1] (henceforth termed the "Space Fence") involves searching for radar returns from spacecraft. A large region of sky (e.g., $> 90°$) may need to be searched efficiently.

More recently, Cornwell (2004a) has extended the work by Carter (1988), making use of the w-projection methodology (Cornwell et al., 2008). Briefly, the measured visibilities or cross-correlations from a radio astronomical interferometer are intrinsically 3-dimensional while the desired sky brightness is a 2-dimensional quantity, i.e., a function of angles or direction cosines. In standard (far-field) radio astronomical processing, particularly for narrow fields of view, one can approximate the measured visibilities by a 2-dimensional quantity and then use a Fourier transform relation to obtain the sky brightness. This approximation is equivalent to assuming that the interferometer is essentially *planar*. The w-projection relaxes these approximations by making use of higher order terms that are neglected during the standard radio astronomy processing. Essentially, the difference between standard far-field and w-projection is that the standard method uses only the Franhaufer term while the w-projection retains a Fresnel term. Using a Fresnel term for w-projection also implies that it might have applicability to near-field imaging over large regions of sky.

This document serves to elucidate various assumptions or steps that Cornwell (2004a) leaves unstated, with the particular aim of applying w-projection to the Space Fence. Throughout we use the same coordinate system (Figure 1) as Cornwell (2004a): The positions of receptors or antennas are denoted by $\mathbf{r}_i$ (i.e., numerical subscripts), the positions of emitters are denoted by $\mathbf{r}_x$ (i.e., alphabetical subscripts), and the direction from the center of the array and the center of the
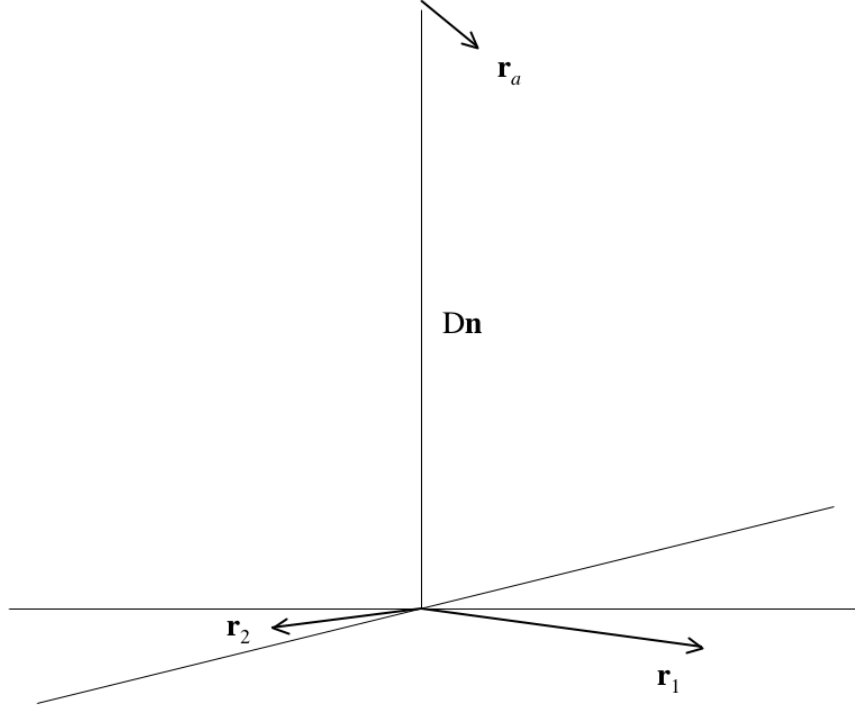
---

[1]This system was formerly known as the Navy Space Surveillance (NAVSPASUR) system.

Fig. 1—Geometry for w-projection. Receptors are located at $\mathbf{r}_1$ and $\mathbf{r}_2$, an emitter is located at $\mathbf{r}_a$, and the distance from the center of the array to the center of the field of view is D. All vectors, $\mathbf{r}_1$, $\mathbf{r}_2$, and $\mathbf{r}_a$, are three-dimensional (i.e., their z components are not assumed to be 0).

(angular) area of regard is $\hat{n}$. The distance from the array of receptors to the mid-point of the area of regard is D. We shall make the restriction that $z_i < D$ and $z_x < D$.

2. PHYSICAL MOTIVATION AND RADIO ASTRONOMY BACKGROUND

We motivate the remainder of this document (as well as the discussions in Carter 1988, Cornwell 2004a, and Cornwell 2004b) by considering a series of increasingly complicated scenarios (viz. Figure 1).

1. The emitter is in the far-field, and area of regard is small. Thus, $D \to \infty$, small-angle approximations can be used (with respect to r_a), and the wavefronts from the emitter can be assumed to be planar across the entire receiving array. This case is the traditional radio astronomical interferometric imaging case (Thompson, Moran, & Swenson, 1986). A fundamental theorem (the van Cittert-Zernike theorem) for this case is that there is a 2-dimensional Fourier relation between the brightness or intensity distribution on the sky and the second moment of the electric field across the receiving array (the *visibility* function). A key assumption of the van Cittert-Zernike theorem is that the receiving array can be assumed to be *planar*.

2. The emitter(s) is in the far-field, but the area of regard is not small. In this case, $D \to \infty$ and the wavefronts *from any particular point in the area of regard* are planar across the receiving array. Effectively, the geometry of the receiving array *as seen from the area of regard* must be taken into account or the *non-coplanar* nature of the receiving array can no longer be neglected. The full three-dimensional characteristics of the visibility function must considered. The w-projection methodology was developed to handle this case for radio astronomical imaging (Cornwell et al., 2008); see also Cornwell & Perley (1992) for alternate approaches to this case.

3. The emitter is no longer in the far-field, but the area of regard is small. In this case, the curvature of the wavefronts across the array must be taken into account, but small-angle approximations can often be retained. This case was considered by Carter (1988).

4. The emitter(s) is no longer in the far field and the area of regard is not small. In this case, both the curvature of the wavefronts from any point in the area of regard and the non-coplanar nature of the receiving array must be taken into account. This case is considered by Cornwell (2004a) and in this document.

Finally, we adopt nomenclature and terminology derived from radio astronomical heritage. Specifically, the *visibility function V* has multiple meanings. From considerations of the van Cittert-Zernike theorem and its extensions to wide-field and near-field imaging, the visibility function can be used to indicate the continuous function defined everywhere in the 3-dimensional volume defined by the receiving array. In general, the receiving array consists of only a finite number of receptors, located at r_i. Thus, the measurements of the visibility function are finite in number and occur only at set of locations defined by the receptor positions $\{r_i\}$, denoted $V(\{r_i\})$. Finally, a specific measurement of the visibility function is determined by any two receptors, denoted $V(r_i, r_j)$.

3. "GEOLOCATION AS A SEARCH TECHNIQUE"

Cornwell (2004a) casts geolocation as a search technique for finding the source(s) of emission from the received voltage streams from an array of antennas. The "visibility" for a pair of antennas at $\mathbf{r}_1$ and $\mathbf{r}_2$ for an emitter $\mathbf{r}_a$ is

$$V(\mathbf{r}_1, \mathbf{r}_2) = \int I_a g_1^a g_2^a \, d\mathbf{r}_a, \tag{3.1}$$

where g_i^a is the Green's function for the propagation from emitter a to the receptor i (Cornwell, 2004a, equation 15).

The Green's function for the propagation of the radiation from emitter a to receptor 1 is (Jackson, 1975, Chapter 6)

$$g_1^a = \frac{1}{|\mathbf{r}_a - \mathbf{r}_1 + D\hat{n}|} \exp(ik|\mathbf{r}_a - \mathbf{r}_1 + D\hat{n}|). \tag{3.2}$$

Here $k \equiv 2\pi/\lambda$ is the wavenumber.

Expansion of the product of the Green's functions (Cornwell, 2004a, equation 18) yields, to first order,

$$V(\mathbf{r}_1, \mathbf{r}_2) = \int f(\mathbf{r}_1, \mathbf{r}_2; \mathbf{r}_a; D) I_a \exp[ik(r_1^2 - r_2^2)/2D - ik(\mathbf{r}_1 - \mathbf{r}_2) \cdot \mathbf{r}_a/D] \, d\mathbf{r}_a \tag{3.3}$$

(cf. Cornwell, 2004a, equation 19). Here $f(\mathbf{r}_1, \mathbf{r}_2; \mathbf{r}_a; D)$ is a function that incorporates the amplitude factor from the Green's functions.

The traditional (u, v, w) coordinate system of radio astronomy has $\mathbf{u} \equiv k(\mathbf{r}_1 - \mathbf{r}_2)/2\pi$. In standard, far-field radio astronomical imaging, a "direction cosines" coordinate system is used in which $\tan \ell \sim \sin \ell \sim \ell \sim x_a/D$ and $\tan m \sim \sin m \sim m \sim y_a/D$. We relax the small-angle approximation here, but to emphasize the similarity with standard radio astronomical imaging, we use the coordinate system $\ell = (\ell, m) \equiv \mathbf{r}_a/D$.

Equation 3.3 can thus be re-written in the suggestive form

$$
\begin{aligned}
V(\mathbf{r}_1, \mathbf{r}_2) &= \int f I_a \exp[ik(r_1^2 - r_2^2)/2D - 2\pi i(u\ell + vm)] \, d\mathbf{r}_a \\
&= \int D f I_a \exp[ik(r_1^2 - r_2^2)/2D] e^{-2\pi i(u\ell + vm)} \, d\ell \, dm.
\end{aligned}
\tag{3.4}
$$

As discussed by Carter (1988), a redefinition of the antenna locations results in the first exponential term, the Fresnel term, disappearing. The redefinition applies to the z coordinate of the antenna locations:

$$
z' = D - \sqrt{D^2 - (x^2 + y^2)}.
\tag{3.5}
$$

Cornwell (2004a) calls this coordinate redefinition "Carter refocussing."

Cornwell (2004a) continues to expand the phase term of the Green's function product (eqns. [3.2] and [3.3]) to second order (see Cornwell, 2004b). After "Carter refocussing" coordinate redefinition, the result is

$$
\begin{aligned}
V(\mathbf{r}_1, \mathbf{r}_2) &= \int f I_a \exp[-ik(\mathbf{r}_1 - \mathbf{r}_2) \cdot \mathbf{r}_a/D] \exp[-ik(r_1^2 - r_2^2)r_a^2/2D^3] \, d\mathbf{r}_a \\
&= \int D f I_a \exp[-ik\{(r_1^2 - r_2^2)/2D\}\{r_a/D\}^2] e^{-2\pi i(u\ell + vm)} \, d\ell \, dm.
\end{aligned}
\tag{3.6}
$$

Equation (3.6) clearly has the form of a 2-dimensional Fourier transform. Further, it is similar in appearance to the radio astronomical w-projection expression (Cornwell et al., 2008, eqns. 10–14). In an effort to make the similarity even more apparent, we write equation (3.4) as[2]

$$
\begin{aligned}
V(\mathbf{r}_1, \mathbf{r}_2) &= \int N(r_1, r_2; D) \, (D f I_a) \, e^{-2\pi i(u\ell + vm)} \, d\ell \, dm \\
&= \tilde{N}(r_1, r_2; D) \otimes V(\mathbf{r}_1, \mathbf{r}_2 | z_1 = 0, z_2 = 0).
\end{aligned}
\tag{3.7}
$$

where $\otimes$ is the convolution operator.

4. DEPTH OF FOCUS

Using the equivalent of the w-projection term, in the N function, we can expand the phase term to obtain an estimate of the depth of focus or the range in distance D over which equation (3.7) applies. Equivalently, this "depth of focus" also implies an angular distance over which

---

[2]While Cornwell (2004a) uses G to denote the convolution function, we prefer N, both to distinguish it from the original Green's functions as well as to emphasize the near-field aspects.

equation (3.7) applies. Consider an emitter at position $\mathbf{r_a}$ (Figure 1), such that it is perpendicular to $D\hat{n}$ (i.e., $z_a = 0$). This emitter can be considered to be either at an angular offset, with a direction cosine given by r_a/D or at a distance $\sqrt{r_a^2 + D^2}$. (The latter also implies a different $\hat{n}$.)

We begin with just the phase term

$$k\frac{r_1^2 - r_2^2}{2D}\left(\frac{r_a}{D}\right)^2 = k(r_1^2 - r_2^2)q^2/2D, \tag{4.1}$$

where $q^2 \equiv \ell^2 + m^2$ (Cornwell, 2004a, eqn. 25). The quantity $\sqrt{r_1^2 - r_2^2}$ can be no larger than the maximum baseline in the array, and we shall approximate $r_1^2 - r_2^2 \sim B^2$. Further, the Fresnel zone is defined as $R_F \equiv \sqrt{\lambda D}$.

We define the depth of focus as the change in the distance D that produces a phase change of order 1 radian. Letting $D \rightarrow D + \Delta D$ in equation (4.1), expanding to lowest order in $\Delta D/D$, and setting the resulting perturbation term equal to unity, algebraic manipulation yields

$$\Delta D \sim \left(\frac{D}{B}\right)^2 \left(\frac{R_F}{r_a}\right)^2 D. \tag{4.2}$$

Physically, the depth of focus is related to two factors. The first is related to the size of the array relative to the distance to the target D/B. The second is related to the size of the area being imaged relative to the size of the Fresnel zone R_F/r_a.

5. IMPLEMENTATION

As Cornwell (2004a) describes, the equivalent convolution function can be written as a Hankel transform. In order to make this explicit, we express the convolution function as

$$\begin{aligned}
\tilde{N} &= \int \exp[ik(r_1^2 - r_2^2)q^2/2D]e^{2\pi i(ul+vm)}\,dl\,dm \\
&= \int \exp[ik(r_1^2 - r_2^2)q^2/2D]e^{2\pi iqb(\cos\chi\cos\psi+\sin\chi\sin\psi)}\,dq\,d\chi.
\end{aligned} \tag{5.1}$$

Here we express the array baselines (u, v) and the target direction cosines (l, m) in a polar coordinate system, $(u, v) = (b\cos\psi, b\sin\psi)$ and $(l, m) = (q\cos\chi, q\sin\chi)$. Using trignometric identies, we can perform one of the integrations (over χ), leaving

$$\tilde{N} = \int \exp[ik(r_1^2 - r_2^2)q^2/2D]J_0(2\pi qb)\,q\,dq, \tag{5.2}$$

where $J_0(x)$ is the zeroth-order Bessel function. The left-hand side of equation (5.2) is now in the form of a zeroth-order Hankel transform of the (radially-symmetric) function $\exp[ik(r_1^2 - r_2^2)q^2/2D]$. Implementations of the Hankel transform are available.[3]

An important point, though often left implicit in Cornwell (2004a), is that the visibilities are expressed in terms of the sky brightness. For a given sky brightness, one can Fourier transform (2-dimension) to obtain the visibility function, then w-project it to form the full, 3-dimensional

---

[3]e.g., http://wwwuser.gwdg.de/%7Emleuten/MATLABToolbox/HankelTransform.html

visibility function. This process is limited only by numerical errors (Cornwell et al., 2008). For imaging, we have measured the visibilities and desire the (unknown) sky brightness.

We return to equation (3.7). Generally, one would like to use a Fast Fourier transform (FFT) to obtain the image I from the visibility V. In the radio astronomical case, the visibility data are gridded onto a uniform grid in order to enable the FFT. Consequently, we now discuss the implementation in matrix form.

$$\begin{aligned} V(\mathbf{r}_1, \mathbf{r}_2) &= \tilde{N}(r_1, r_2; D) \otimes V(\mathbf{r}_1, \mathbf{r}_2 | z_1 = 0, z_2 = 0) \\ \tilde{N}^{\mathrm{T}} V(\{\mathbf{r}_i\}) &= \tilde{N}^{\mathrm{T}} \tilde{N} \otimes V(\{\mathbf{r}_i\} | \{z_i = 0\}). \end{aligned} \tag{5.3}$$

For a unitary matrix, $\tilde{N}^{\mathrm{T}} \tilde{N} = \mathbf{I}$, implying that the r.h.s. of eqn. (5.3) reduces to just $V(\{\mathbf{r}_i\} | \{z_i = 0\})$.

Implementation of near-field w-projection thus involves the following steps, for a given array. We assume that the antenna locations $\mathbf{r}_i$ are known and that the array output are the visibilities $V(\mathbf{r}_i, \mathbf{r}_j)$ for all unique pairs.

1. Choose a distance at which the target is known or suspected to be. This distance should be informed by the depth of focus (§4).

2. Compute the transpose matrix $\tilde{N}^{\mathrm{T}}$. This matrix is *independent* of the visibility data, so that for an array with fixed antenna positions, pre-computation of this matrix is possible.

3. Grid the observed three-dimensional visibilities. In the radio astronomical case, this is performed via a multiplication of the observed visibilities by a *gridding convolution function*. The gridding convolution function is chosen to have a small support, and the gridded visibility function can be easily resampled on a uniform grid. Again, it may be possible for this function to be pre-computed.

4. Multiply the observed (and gridded) visibilities by the $\tilde{N}^{\mathrm{T}}$ matrix to produce the w-projected visibilities.

5. Perform a 2-dimensional transform of the near-field w-projected visibilities to obtain the sky brightness.

As Cornwell (2004a) and Cornwell et al. (2008) discuss, depending upon the complexity of the sky brightness, additional processing steps can be conducted such as deconvolution (e.g., CLEAN).

6. APPLICATION OF NEAR-FIELD W-PROJECTION IMAGING TO THE SPACE FENCE (AFSSS)

In this section we illustrate the use of near-field w-projection using the Space Fence receiving arrays. Briefly the receiving arrays consist of St. Andrew's crosses with a maximum east-west (E-W) baseline of 1600 ft. (488 m) and a maximum north-south (N-S) baseline of 1200 ft. (366 m). The observation frequency is 216.98 MHz, producing an angular resolution in the E-W direction of 3.4 milliradians (11.7′) and in the N-S direction of 4.5 milliradians (15.6′). Using equation (11) from Carter (1988), the far field is at least 1100 km distant for the E-W baselines and 600 km distant for

Fig. 2—The Long Wavelength Demonstrator Array. The dipoles are in the foreground and are approximately 1 m high. The LWDA electronics are housed in the shed in the background. The operational frequency range is 60–80 MHz. Antennas of the the Very Large Array (VLA) are in the background.

the N-S baselines. For additional details about the Space Fence transmitting and receiving arrays, see Meekins (1988) and Solomon (1990).

We begin by illustrating the concept of using imaging with a phased dipole array to localize emitters within the field of view. NRL has implemented the Long Wavelength Demonstrator Array (LWDA), an array of 16 dipoles located in central New Mexico[4] and operating over the frequency range 60–80 MHz (Figure 2). The array is designed as a testbed for radio astronomical observations, with a pseudo-random distribution of dipoles and an operational frequency range chosen to be compatible with one of the operational frequencies for the nearby Very Large Array (VLA).

It has long been known that as a meteor enters the Earth's atmosphere, its velocity is high enough that it can produce a ionized trail, which can reflect a transmitted RF signal (e.g., Millman et al., 1948). In 2006 November, the LWDA acquired data at a frequency of 61 MHz during the Leonid meteor shower. This frequency was chosen to be one at which a number of TV stations in New Mexico and the southwest U.S. transmit. Figure 3 illustrates two examples of a meteor reflection imaged by the LWDA.

LWDA imaging of meteor trail reflections bears obvious similarities to the Space Fence receiving sites. Both are phased dipole arrays, with operational frequencies differing by a factor of only 3.6, and both can image the reflection of a signal from a distant transmitter. Because it is intended to test radio astronomical hardware and software, the LWDA images are formed by Fourier transforming the visibility data (phase differences) from unique dipole pairs. Even for reflections from meteor trails, this far-field imaging approach is sufficient as the far-field distance is at an altitude of merely 0.5 km. In contrast, the higher frequency and larger size of the Space Fence receiving

---

[4]Latitude: 34.076N, Longitude 107.618W; west of the city of Socorro, NM

Table 1—Space Fence Depth of w-projection Focus (E-W)

Transverse distance (km)	300 km altitude			1000 km altitude		
	Angle (rad.)	Field of View (°)	ΔD (km)	Angle (rad.)	Field of View (°)	ΔD (km)
10	0.03	3	300	. . .	. . .	. . .
30	0.10	11	300	0.03	3	1000
100	0.33	38	300	0.10	11	1000
300	1.00	115	300	0.30	38	1000
445	1.48	170	238	. . .	. . .	. . .
1000	. . .	. . .	. . .	1.00	115	1000
1483	. . .	. . .	. . .	1.48	170	1000

arrays means that the far-field distance is at a higher altitude and near-field effects must be taken into account in making the images.

Table 1 summarizes the depth of focus (equation 4.2) for the Space Fence receiving (east-west) arrays for satellites at two different altitudes. Several comments are warranted about this table. First, many of the depth of focus values ΔD are equal to the assumed altitude D. This equality is the result of our assumption in deriving eqn. (4.2) that ΔD is "small" so that an expansion in terms of $\Delta D/D$ is valid. Allowing $\Delta D/D \to 1$ may seem to violate this assumption, but we have made other approximations (e.g., $r_1^2 - r_2^2 \sim B^2$) that are conservative.

Second, examination of Figure 1 shows that the depth of focus applies to an angular displacement from the center of the field (r_a/D). Consequently, the full field of view (Columns 3 and 6) or the area that can be imaged with one depth of focus correction is twice the angular displacement. Further, anticipating the use of the Space Fence to large fields of view, we extend the list of transverse displacements to correspond to an angular displacement of 1.48 radians (85° off zenith, or a field of view of 170°).

Our interpretation of these values is the following. At altitudes of about 1000 km, the depth of focus for w-projection imaging is comparable to the altitude, even for large fields of view. Thus, a single w-projection should be able to image most of the near-field region. The one exception would be for low-altitude satellites ($\lesssim$ 300 km) at large angles off zenith. For these directions, one may need to refocus the array (i.e., choose a different direction for $\hat{n}$, which in turn implies a different set of $[u, v, w]$).

A nominal CONOPS for near-field w-projection imaging with the Space Fence is thus the following. Phase data are acquired as in current standard operating procedure. Visibility data[5] (i.e., correlation coefficients) are constructed by determining the phase differences between the unique pairs of antennas, relative to a (arbitrary) reference antenna. The visibility data are then processed in two separate methods or "streams" (which could clearly be conducted in parallel):

---

[5]In general, visibility data are complex, having amplitude and phase or real and imaginary components. In practice, for the Space Fence, only the phase data are measured, and it is sufficient to choose a nominal, constant amplitude for all antennas.

Near-field The prescription of Section 5 is used, e.g., with a target altitude of 1000 km. In particular, because one depth of focus is sufficient and the positions of the Space Fence receiving array elements are fixed, Steps #1 and #2 can be precomputed (e.g., stored in a look-up table). Further, the gridding function of Step #3 could also be precomputed.

Far-field The visibility data are gridded and transformed (FFT). Again, because the positions of the receiving arrays are fixed, the gridding function could be precomputed.

The output of either processing stream would be an *image*, showing energy as a function of position above the array (Figure 3). The image is effectively a 2-dimensional matrix, the elements of which encode the direction cosine information to any radar reflections within the field of view. Quality control checks can be performed on such an image.[6] An image that passes the quality control check(s), could then be scanned in an automatic manner for any energy intensity peaks representing reflections from satellites passing through the Space Fence beam. The position of the intensity peaks would then be extracted from the image and used to report satellite positions.

Finally, we note a curious fact about near-field processing for the Space Fence. One of the original motivations for the *w*-projection technique was that radio astronomical interferometers are not, in general, coplanar, because of local topology, the array is large enough that the radius of the Earth has to be taken into account, or both. The Space Fence *is* coplanar (Solomon 1990; E. Lydick 2009, private communication), but, in order to use it for near-field imaging, it must be transformed into a non-coplanar array (viz. the discussion concerning eqn. [3.5]).

---

[6]For example, a standard radio astronomical test is to measure the value of the rms pixel intensity in the image. Only images with rms pixel intensity values lower than some threshold are considered viable for further processing.
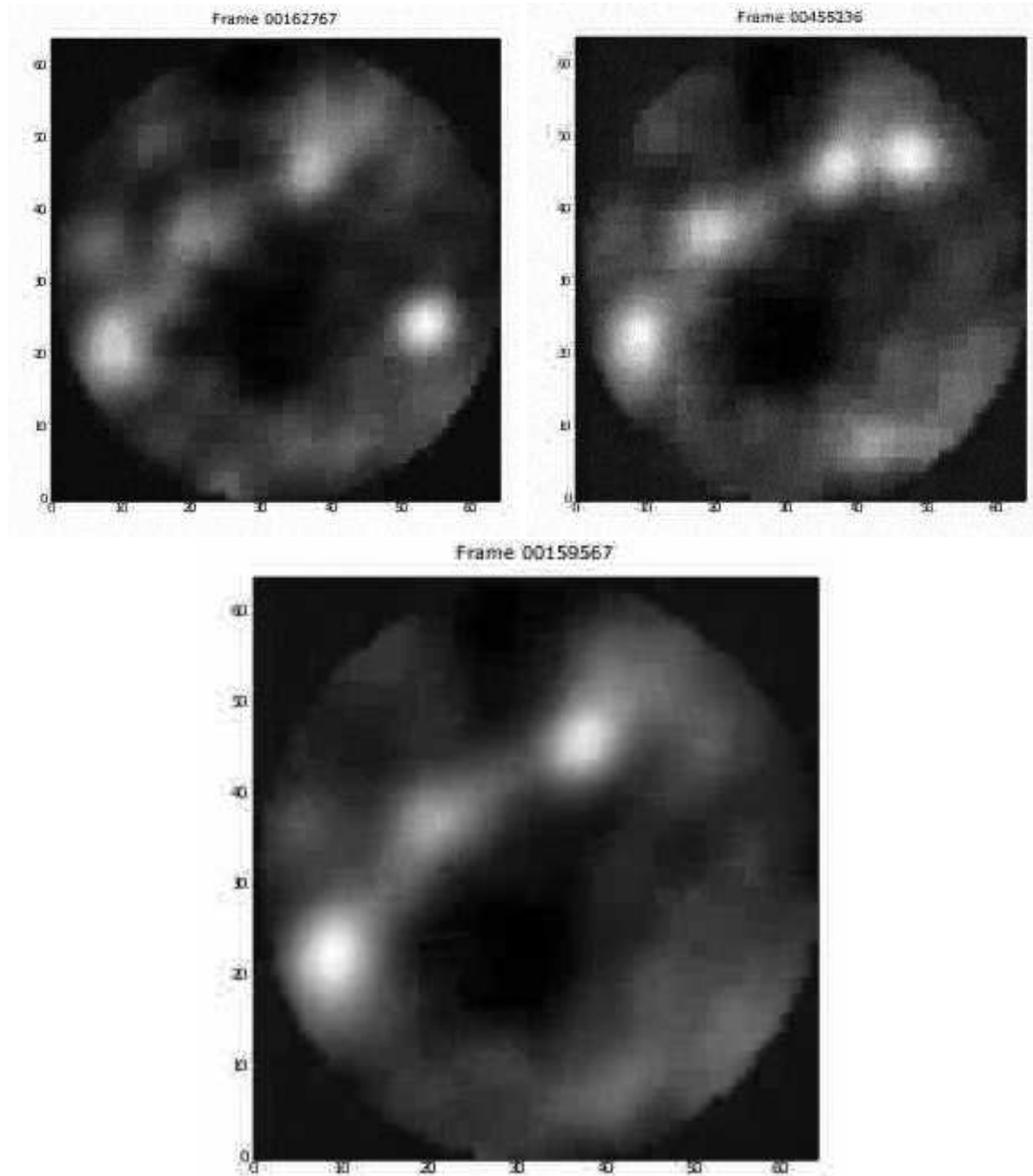
Fig. 3—LWDA images of reflected TV signals from ionized meteor trails during the 2006 Leonid meteor shower. Each image is constructed from a 0.1 s data acquisition at a frequency of 61 MHz. (*Top Left*) and (*Top Right*) Images of reflected signals from Leonid meteors. (*Bottom*) A reference image showing the nominal sky observed by the LWDA. The zenith is at the center of the image. The two discrete emitters near the center of the field are celestial radio sources (Cas A and Cyg A). The band of emission stretching from the upper right to lower left, terminating in the strong emitter near the edge of the field is from the Milky Way Galaxy.

7. BIBLIOGRAPHY

Black, G., Campbell, D. B., Treacy, R., & Nolan, M. C. 2005, "Radar-Interferometric Asteroid Imaging Using a Flexible Software Correlator," Bull. Amer. Astron. Soc., 37, 1155

Carter, W. H. 1988, "Refocusing a Radio Telescope to Image Sources Within the Nearfield of the Antenna Array," NRL Report 9141

Cornwell, T. J. 2004a, "The Correction of Near Field Effects in Radio Interferometric Geolocation"

Cornwell, T. J. 2004b, "Approximate Formulas for the Distance Term in Far and Near Field Interferometery," EVLA Memo 75; `http://www.aoc.nrao.edu/evla/memolist.shtml`

Cornwell, T. J., Golap, K., & Bhatnagar, S. 2008, "The Non-coplanar Baselines Effect in Radio Interferometry: The W-Projection Algorithm," IEEE J. Selected Topics Signal Proc., 2, 647

Cornwell, T. J., & Perley, R. A. 1992, "Radio-Interferometric Imaging of Very Large Fields — The Problem of Non-Coplanar Arrays," Astron. & Astrophys., 261, 353

Jackson, J. D. 1975, *Classical Electrodynamics* (Wiley: New York)

Meekins, J. F. 1988, "Present Radar Fence System Model: Interferometry Techniques Series No. 3" NRL Memorandum Report 6375

Millman, P. M., McKinley, D. W. R., & Burland, M. S. 1948, "Combined Radar, Photographic and Visual Observations of the Perseid Meteor Shower of 1947," Nature, 161, 278

Solomon, D. 1990, "NAVSPASUR Direction Cosine Processing," report for NRL

Thompson, A. R., Moran, J. M., Swenson, G. W. 1986, *Interferometry and Synthesis in Radio Astronomy* (Wiley-Interscience: New York)